Applied Geochemistry 86 (2017) 49–58

Contents lists available at ScienceDirect

Applied Geochemistry

journal homepage: www.elsevier.com/locate/apgeochem

A hydrogeochemistry and multi-isotope (Sr, O, H, and C) study of groundwater salinity origin and hydrogeochemcial processes in the shallow confined aquifer of northern Yangtze River downstream coastal plain, China

Qi Zhao [a, b], Xiaosi Su [a, *], Bo Kang [c], Yan Zhang [d], Xiancang Wu [e], Mingyao Liu [d]

[a] College of Construction Engineering, Jilin University, Changchun 130021, China
[b] Department of Municipal and Environmental Engineering, Taiyuan College, Taiyuan 030000, China
[c] School of Natural Resources and Environmental Engineering, Hefei University of Technology, Hefei 230009, China
[d] Geological Survey of Jiangsu Province, Nanjing 210018, China
[e] Shandong Geological Engineering Investigation Institute, Jinan 250014, China

ARTICLE INFO

Article history:
Received 22 May 2017
Received in revised form
23 September 2017
Accepted 27 September 2017
Available online 28 September 2017

Editorial handling by Dr. I. Cartwright.

Keywords:
Coastal confined groundwater
Salinity
Hydrogeochemcial processes
Multiple environmental tracers

ABSTRACT

Economically developed coastal areas have a high water demand, and their groundwater resources can be threatened by salinization. Many methods and tracers have been used to discriminate the source of salinization because a single method does not yield reliable results. In this paper, the shallow confined coastal plain aquifer, north of the downstream Yangtze River in China, is used as a case study to investigate the origin of the salinity and the relevant geochemical processes for this aquifer. Multiple environmental tracers of major ions, minor ions (Br^-, I^-), and isotopes (^{18}O, ^{2}H, ^{13}C, ^{87}Sr, ^{3}H, ^{14}C) were used so as to provide reliable conclusions. The TDS distribution of the aquifer has an increasing trend, from below 500 mg/L in the inland areas to more than 20,000 mg/L around the southeast coastline. The water chemical type evolves from HCO_3-Ca to Cl-Na as the TDS increases. The results suggest that the groundwater salinity is influenced by seawater intrusion. The seawater proportions in the groundwater samples range from 0.07% to 94.41% and show the same spatial distribution pattern as TDS. The ^{3}H and ^{14}C values show that the highest salinity was mainly caused by a seawater transgression around 6000a B.P. The aquifer is also affected by other hydrogeochemical processes: base exchange has enriched Ca^{2+} and depleted K^+ and Na^+, sulfate reduction has reduced the concentration of SO_4^{2-} and enriched HCO_3^-, and iodine-rich organic matter decomposition has enriched the concentration of I^-. The iodine enrichment also suggests paleo-seawater intrusion. In addition, the precipitation of carbonate minerals has decreased the concentration of Ca^{2+}, Mg^{2+}, and HCO_3^-, albeit to a limited extent.

1. Introduction

Economically developed and densely populated coastal areas have been experiencing a large groundwater demand from agricultural, industrial, and domestic requirements (Trabelsi et al., 2007) and can have many geo-environmental problems. In recent years, groundwater salinization has become an increasing threat to water resources in many coastal areas.

Many studies have addressed the origin of coastal groundwater salinity (e.g. Custodio, 2010; Moussa et al., 2011; Cary et al., 2015; Santucci et al., 2016). Various saline sources were identified, such as modern and paleo-seawater intrusion (de Montety et al., 2008; Han et al., 2011; Wang and Jiao, 2012), evaporitic rock dissolution (Mongelli et al., 2013; Brenot et al., 2015), overlying or underlying salt water (TDS>1000 mg/L) intrusion (Khaska et al., 2013; Eissa et al., 2016), evapotranspiration (Herczeg et al., 2001), and anthropogenic pollution (Ghabayen et al., 2006; Hamouda et al., 2011). Of these sources, seawater intrusion occurs globally (Werner et al., 2013). The increase in chloride concentration in groundwater is a distinctive characteristic of seawater intrusion, and chloride behaves as a conservative substance. Analyses of the relationship between chloride and major ions, ^{18}O, and ion ratios (Br/Cl and Na/Cl for example) are the most common methods used

* Corresponding author.
E-mail address: suxiaosi@163.com (X. Su).

https://doi.org/10.1016/j.apgeochem.2017.09.015
0883-2927/

to identify seawater intrusion (de Montety et al., 2008; Han et al., 2011; Wang and Jiao, 2012; Chandrajith et al., 2013; Santucci et al., 2016). However, sources and processes other than seawater intrusion can also make the above mentioned components have marine like characteristics. One example is evaporation. Therefore, researchers have sought tracers that do not deviate in chemical reactions and biological processes. Strontium isotopes have these characteristics (Cartwright et al., 2007). Seawater has a relatively constant $^{87}Sr/^{86}Sr$ ratio (Vengosh et al., 2002) and thus groundwater affected by seawater intrusion would have a marine $^{87}Sr/^{86}Sr$ ratio. In addition, different minerals have distinct ranges of $^{87}Sr/^{86}Sr$ ratios, and groundwater interacting with these minerals shows corresponding ranges of $^{87}Sr/^{86}Sr$ ratios (Cartwright et al., 2007). These characteristics make strontium isotopes effective tracers for seawater intrusion and water-rock interaction (Jørgensen et al., 2008; Bakari et al., 2013; Khaska et al., 2013; Szynkiewicz et al., 2014; Cary et al., 2015; Petelet-Giraud et al., 2016).

Coastal aquifers can be subjected to multiple phases of seawater transgression and regression in different geological periods, which makes it important to distinguish between modern and paleo-seawater intrusion (Werner et al., 2013; Colombani et al., 2017). However, the methods thus far described cannot differentiate effectively between changes in groundwater chemistry caused by ancient and modern seawater intrusions. Radioactive isotopes of ^{3}H and ^{14}C are extensively used to assess groundwater age and to differentiate paleo-groundwater from modern groundwater (Edmunds, 2001; van Geldern et al., 2014). Thus, the ^{3}H and ^{14}C age of the saline groundwater can be used to indirectly distinguish between modern and ancient seawater intrusion (Yechieli et al., 2008; Wang and Jiao, 2012). Iodine is present in sea water with concentrations of around 55 μg/L (Moran et al., 2002). Much higher concentrations are found, and with relative enrichment respective to seawater, in some marine formation water (Moran et al., 2002). Although iodine is suitable for distinguishing the salinity of groundwater from ancient and modern seawater, it is rarely used for this purpose (Sukhija et al., 1996).

Research in China on paleo-seawater intrusion has been confined to the Laizhou Bay in northern China and the Pearl River Delta in southern China. Little research has been done in the central coastal regions, such as the Yangtze River delta (Shi and Jiao, 2014). In this paper, we combine the methods mentioned above so as to distinguish between modern and paleo-seawater intrusion in the coastal plain area of the Yangtze River. The methodology used here can be applied to other similar areas to trace the salinity of groundwater in coastal areas.

The shallow confined aquifer (SCA) in the coastal plain north of the Yangtze River in China contains large amounts of groundwater. However, it is undeveloped because the groundwater has high TDS concentrations. Interest in the development of this aquifer has arisen in response to the dramatic increase in water demand and the limited availability of other sources. However, studies on this aquifer, especially on the origin of groundwater salinity, are relatively scarce. It is difficult to delineate seawater intrusion and relative processes because of the long residence times and abundant organic matter (de Montety et al., 2008; Wang and Jiao, 2012) in confined aquifers. Thus, it is a major research challenge to assess the marine influence on confined groundwater.

In this study, we aim to investigate the origins of groundwater salinity in a SCA and identify the major hydrogeochemical processes controlling its chemistry using stable and radioactive isotopes (^{18}O, ^{2}H, ^{13}C, ^{87}Sr, ^{3}H, ^{14}C), major ions, and trace elements (Br, I). We believe this study will provide useful insights for other regions, both in China and globally, with similar hydrogeological conditions.

2. Study area

The study area is the coastal plain north of the Yangtze River in China. To the east of the study area is the Yellow Sea, and to the south is the Yangtze River (Fig. 1). The study area has an average temperature of 15.2 °C, a mean annual rainfall of 1050.8 mm, and an average annual evaporation of 877.2 mm. The Yangtze River is the most important river in the study area and has a width of 5–10 km.

The climate of the Quaternary has exhibited dramatic changes, with characteristic alternating cold and hot periods. The study area has experienced many marine transgressions (Table 1) since the Middle Pleistocene. The largest scale transgression occurred around 6000 years ago, and caused the whole study area to be inundated by seawater.

The study area is underlain by a multilayer sequence of unconsolidated, predominantly sand and gravel aquifers separated by silt and clay confining units. As a result of the burial conditions and water-bearing zones, the unconsolidated aquifer can be divided into unconfined and confined aquifers. The confined aquifer can be further divided into a shallow and a deep confined aquifer with distinct deposition times, depths, and hydraulic properties. The SCA is the focus of this study.

The SCA lies at a depth of 40–60 m below the land surface, and has an average thickness of 100 m. The aquifer comprises late to middle Pleistocene marine and alluvial/fluvial deposits of fine to coarse sand and gravels (Fig. 1S). A continuous impermeable clay layer overlies the aquifer separating it from the unconfined aquifer (UA for short). Between the shallow and deep confined aquifer is a continuous clay layer with a thickness of up to 30 m in most parts of the study area. Thus, the hydraulic connection between the shallow and deep confined aquifers is minimal. The shallow confined water (SCW) is flowing from inland to the sea with an average flow velocity of 3 mm/d (Fig. 1).

3. Materials and methods

3.1. Sampling

Because most of the groundwater in the study area is highly saline, there are a few available supply wells for hydrogeochemical monitoring. Therefore, additional observation wells had to be established, and a total of 20 wells were drilled for the purpose of this study. To fully understand local geological and hydrogeological conditions, 30 representative groundwater samples from production wells and observation wells (Fig. 1) were taken from the SCA in November to December 2014. One Yellow Sea water sample and four Yangtze River water samples were also collected (Fig. 1). All collected water samples were filtered through a 0.45 μm membrane and then stored at 4 °C in tightly capped HDEP bottles. Water samples for cation analysis were acidified using analytically pure nitric acid to pH < 2.

3.2. Analytical techniques

Temperature and pH were directly measured in situ using portable meters. Alkalinity was measured by titration with HCl (0.025 mol/L) on the day of sampling. The measurement of major ions was performed at Nanjing Mineral Resources Supervision and Testing Center. The concentrations of Na^{+}, K^{+}, Ca^{2+}, Mg^{2+}, and SO_4^{2-} were analyzed using inductively coupled plasma atomic emission spectrometry (ICP-AES). Concentrations of Cl^{-} were determined by titration with $AgNO_3$. The concentrations of Br^{-} and I^{-} were analyzed using inductively coupled plasma mass spectroscopy (ICP-MS), and NO_3^{-} values were determined using spectrophotography. The Sr^{2+} concentrations were analyzed with a NexION300D plasma

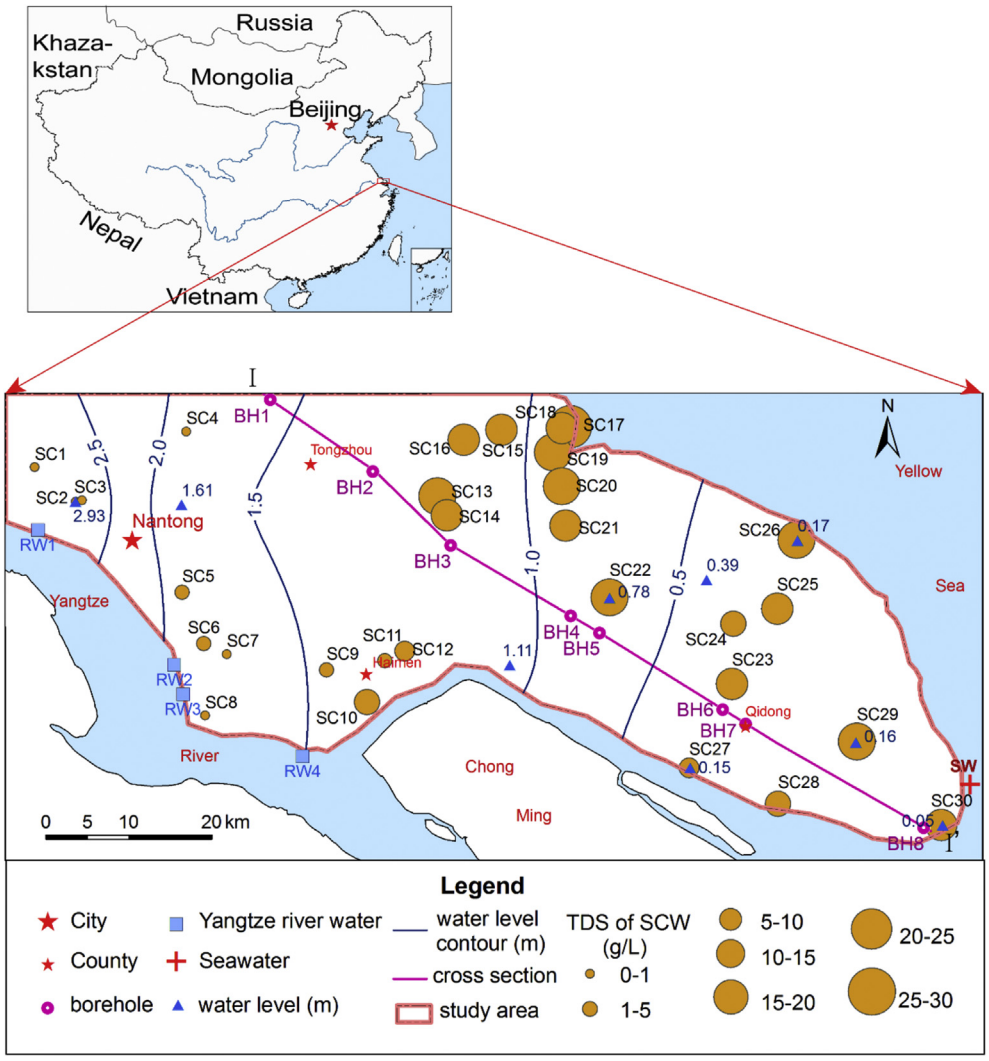

Fig. 1. Location of the SCA in the study area, showing the sampling sites, groundwater flow direction, and TDS distribution.

Table 1
Time and scale of Quaternary seawater transgressions in the study area.

Transgression Time	Transgression Scale
Early stage of Middle Pleistocene	The southeastern part of the study area
Early stage of Late Pleistocene	The whole study area
Late stage of Late Pleistocene	The whole study area
Holocene, about 12000 years ago	The eastern part of the study area
Holocene, about 6000 years ago	The whole study area

mass spectrometer. The analytical precision of the anion and cation measurements, based on replicate analyses, was ±2%. Charge balances for the measured water samples were all within ±5%.

The analyses of $\delta^{18}O$ and δD values were carried out at the China University of Geosciences (Wuhan) using a Picarro L1102-I Laser isotopic analyzer. The $\delta^{18}O$ and δD values were expressed in δ (‰) notation and calculated with respect to VSMOW. The analytical precision for δD was ±1‰ and for $\delta^{18}O$ was ±0.2‰. The ^{3}H level was determined at the Groundwater, Mineral Water, and Environment Monitoring Center of the Ministry of Land and Resources in Shijiazhuang, China using a 1220 Quantulus ultra-low-level liquid scintillation spectrometer. The ^{3}H level was expressed in TU. The detection limit was 2 TU. The analyses of ^{13}C isotopic data and ^{14}C activity were performed at the Beta Analytic-Radiocarbon Dating Laboratory, Miami by the Isotope Ratio Mass Spectrometry and Accelerator Mass Spectrometry methods, respectively. The ^{14}C results were reported as percent modern carbon (pMC) relative to 95% of the ^{14}C activity of oxalic acid, according to SRM 4990C-Oxalic Acid of the National Institute of Standards and Technology. Measured $^{13}C/^{12}C$ ratios ($\delta^{13}C$) were calculated relative to the PDB-1 standard. The precision (1σ) for $\delta^{13}C_{DIC}$ (DIC refers to dissolved inorganic carbon) was ±0.3‰. The ^{14}C detection limit was 0.3 pMC.

The $^{87}Sr/^{86}Sr$ ratio was measured at the Analytical Laboratory of the Beijing Research Institute of Uranium Geology using a thermal ionization mass spectrometer. The $^{88}Sr/^{86}Sr$ ratio was normalized to 8.37521. Measurements of the standard SRM 987 gave $^{87}Sr/^{86}Sr$ ratios of 0.710260 ± 0.000009 (1σ).

4. Results

4.1. Chemical characteristics

The TDS of water samples from the SCW was 366–26570 mg/L. Except in the northwestern and southwestern parts of the study area, the SCW is salt water (TDS>1000 mg/L) in the most of study area (Table 1S and Fig. 1). The horizontal distribution of TDS for the SCW increases along the flow path: the closer it is to the Yellow Sea,

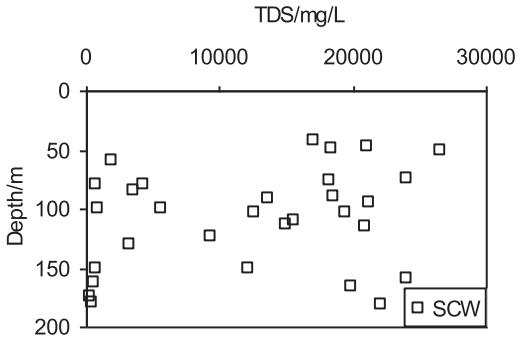

Fig. 2. Relationship between TDS and sampling depth.

the greater the content of TDS. The vertical distribution of TDS is shown in Fig. 2. The TDS of SCW samples do not show a preferential trend with sampling depth ($R = 0.25$, $n = 30$). Fresh and salt water are found at different depths with no obvious salinity stratification.

The SCW water chemical type varies from HCO_3-Na or HCO_3-Na·Ca to Cl-Na as TDS increases (Fig. 2S, indicated by arrows). The pH for the SCW is 6.7–8.5. The NO_3^- concentration of the SCW is < 0.2–5.56 mg/L, which is below the drinking water limit of 50 mg/L (WHO, 2011) and indicates little anthropogenic influence on the water quality.

4.2. Ionic relationships

To understand the relationship between different chemical compositions, Pearson correlation coefficients for the major ions and TDS were calculated. The results are shown in Table 2. Among the major ions, chloride concentration is most strongly correlated with that of TDS. Chloride is also well correlated ($R > 0.5$) with major cations and sulfate, indicating a common source.

The increasing values of chloride can be caused by evapotranspiration, halite (NaCl) dissolution, and mixing with salt water of marine origin. Because the SCA is deeply buried, the contribution of evapotranspiration to the increases in chloride concentration can be ignored. To trace the salinity source, ionic ratios, such as γNa/γCl and γBr/γCl, which are good tracers of groundwater salinity, can be used (Li et al., 2016). Yellow Sea water has a γNa/γCl and γBr/γCl of 0.85 and 0.0013, respectively. If groundwater was affected by seawater intrusion, then the γNa/γCl and γBr/γCl ratios of groundwater should be close to the marine ratio (Hamouda et al., 2011). If the salinity of groundwater was caused by halite dissolution, the γNa/γCl would be close to 1, and the γBr/γCl ratio would be lower than 0.0001 (Hofmann and Cartwright, 2013).

The γNa/γCl ratio of the SCW is 0.42–3.16, with an average value of 0.98. Fig. 3 shows that as chloride concentrations increase, the γNa/γCl ratio remain close to the seawater and halite dissolution lines. This shows that the increasing chloride values may be caused by seawater intrusion or halite dissolution. The γBr/γCl ratio for the SCW is 0.004–0.0018, with an average value of 0.0012, which is much higher than 0.0001. Therefore, it appears that seawater intrusion was mainly responsible for the chloride increases. However, other sources of Br release, including ploughing and biological activity, may also contribute to the observed changes (Khaska et al., 2013). Therefore, it is necessary to obtain more evidence to confirm seawater intrusion.

Table 2
Pearson correlation coefficient (R) matrix for the SCW.

	TDS	Na^+	K^+	Ca^{2+}	Mg^{2+}	Cl^-	HCO_3^-	SO_4^{2-}
TDS	1.000							
Na^+	0.992**	1.000						
K^+	0.857**	0.903**	1.000					
Ca^{2+}	0.574**	0.473**	0.115	1.000				
Mg^{2+}	0.993**	0.979**	0.833**	0.605**	1.000			
Cl^-	0.999**	0.991**	0.860**	0.571**	0.990**	1.000		
HCO_3^-	0.270	0.345	0.496**	−0.273	0.211	0.286	1.000	
SO_4^{2-}	0.747**	0.698**	0.485**	0.655**	0.776**	0.718**	−0.269	1.000

**Correlation is significant at the 0.01 level (2-tailed), n = 30.

5. Discussion

5.1. Seawater intrusion

5.1.1. $\delta^{18}O$, δD and Sr evidence

5.1.1.1. $\delta^{18}O$, δD evidence. H and O stable isotopes are not influenced by water-rock interactions, making them good tracers for determining the origins of groundwater salinity (Boschetti et al., 2010; Hamouda et al., 2011).

Because of the lack of hydrogen and oxygen isotopic data for precipitation in the study area, the $\delta^{18}O$ and δD observation datasets from the Nanjing station (about 200 km from the study area) was used to establish the Local Meteoric Water Line (LMWL, Fig. 4). The Nanjing station forms part of the International Atomic Energy Agency's Global Network of Isotopes in Precipitation.

$$\delta D = 8.49\delta^{18}O + 17.71‰ \text{ VSMOW } (R = 0.98, n = 58)$$

The slope of the LMWL (8.49) is similar to the Global Meteoric Water Line (GMWL, Fig. 4).

$$\delta D = 8.20\ (\pm 0.07)\ \delta 18O + 11.27\ (\pm 0.65)\ ‰ \text{VSMOW (Rozanski et al., 1993)}$$

Yellow Sea water has $\delta^{18}O$ and δD values of −1.21‰, −8.5‰, and is relatively depleted compared with standard mean ocean water. The average $\delta^{18}O$ and δD values of the Yangtze River water samples are the most depleted: −8.54‰ and −58.8‰, Srespectively (Table 1S).

Fig. 4 shows that the measured values of $\delta^{18}O$ and δD of the SCW samples all plot below the LMWL and GMWL, indicating that the SCW is of meteoric origin. The $\delta^{18}O$ and δD values of two samples located near the Yangtze River (SC5, SC27) were −8.08‰ to −8.39‰ and −60.3‰ to −57.5‰, and are similar to the values of the Yangtze River and the weighted average value of precipitation. This indicates that the SCW can be recharged by the Yangtze River water and by precipitation.

The SCW samples are aligned with a line that has a lower slope than the GMWL and LMWL (Fig. 4). This phenomenon may be the result of evaporation and/or mixing processes. Evaporation can be ruled out because of the depth of the SCA. It is suggested that mixing with an enriched end-member dominates the lower slope. Furthermore, the Yellow Sea water sample point is on the trend line of groundwater samples, reflecting that the seawater is probably the enriched end-member.

5.1.1.2. Sr and $^{87}Sr/^{86}Sr$ evidence. The Sr^{2+} concentration and $^{87}Sr/^{86}Sr$ ratio of the Yellow Sea water sample are 8057 μg/L and 0.709177, respectively. For the SCW, the Sr^{2+} concentration and $^{87}Sr/^{86}Sr$ ratio are 870–8263 μg/L and 0.709212–0.710499, respectively. In the correlation plot of $^{87}Sr/^{86}Sr$ values and Sr^{2+} concentrations, the $^{87}Sr/^{86}Sr$ values of the SCW samples decrease as the Sr^{2+} concentration increases (Fig. 5). This suggests that the salinity of SCW may be of marine origin, and provides additional evidence that evaporation is not involved. However, some SCW sample results lie above the mixing zone, indicating that other

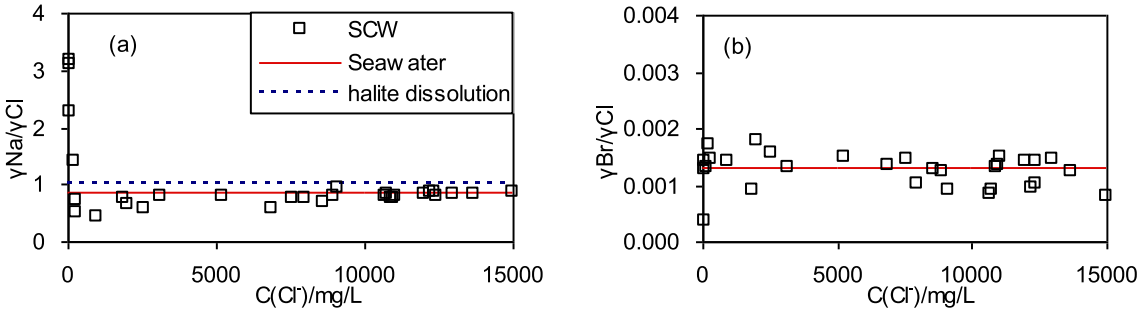

Fig. 3. Relationships between Cl^- and (a) γNa/γCl, and (b) γBr/γCl.

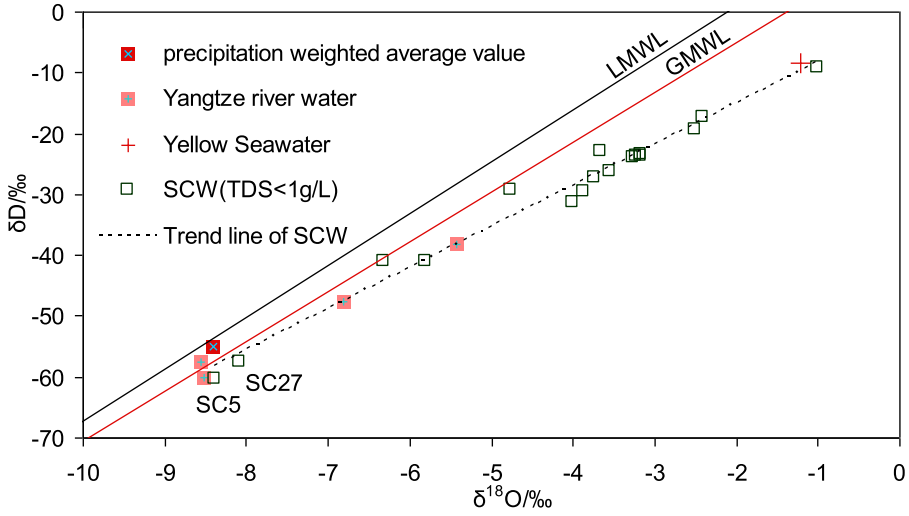

Fig. 4. Values of $\delta^{18}O$ versus δD for various water samples compared with the GMWL and LMWL. The trend line of the SCW water samples is also shown.

processes may have caused changes to the SCW $^{87}Sr/^{86}Sr$ values.

The analysis of $\delta^{18}O$, δD, and Sr suggested that the groundwater was influenced by seawater intrusion. However, the study area has experienced several transgressions since the Middle Pleistocene. Therefore, it is not clear whether the groundwater was affected by modern seawater intrusion or paleo-seawater intrusions. Therefore, further evidence was sought.

5.1.2. Iodine evidence

The SCW has a relatively high iodine concentration, with an average value of 1.3148 mg/L, which is much higher than the Yellow Sea water sample of 0.079 mg/L. Iodine enrichment distinguishes the SCW from seawater, and indicates that modern seawater intrusion has had little impact on iodine deviation.

The SCA experienced multiple phases of paleo-seawater transgressions, making them rich in organisms of marine origin. Some marine organisms, such as algae, assimilate and organically bind iodine in their tyrosine residues, resulting in an a iodine concentration of 30000 times greater than in seawater (Zhang et al., 2013). The iodine-rich organic matter subsequently degrades to release iodine into the water phase, rendering groundwater rich in iodine. Therefore, the high concentration of iodine shows that the paleo-seawater intrusions were the main source of salinity in the SCW.

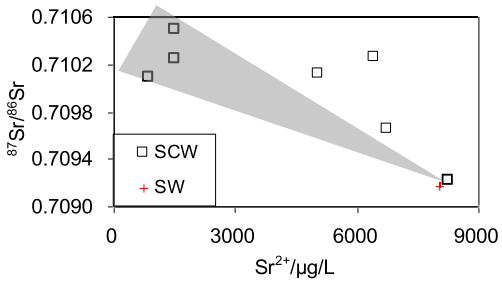

Fig. 5. Relationship between Sr^{2+} and $^{87}Sr/^{86}Sr$.

5.1.3. ^3H and ^{14}C evidence

To provide further evidence for the time of seawater intrusions, radioactive isotopes, ^3H and ^{14}C, are used to calculate the groundwater residence time.

The tritium levels of the SCW samples are all below the detection line of 2 TU (Table 1S), indicating that the SCW was recharged before thermonuclear bomb test era (1960s) (Clark and Fritz, 1997).

Tritium can be used to date young groundwater, but is not suitable for ancient water. For ancient groundwater, ^{14}C is often used for groundwater age dating, and has an upper limit of 30000 years. The ubiquitous presence of DIC in groundwater (Cartwright, 2010) allows radiocarbon dating to be widely applied for deep groundwater residence time assessment. When ^{14}C enters a closed system, it begins to decay. The ^{14}C age of groundwater can be calculated by the following equation:

$$t = \frac{1}{\lambda}\ln\frac{A_0}{A_S}, \lambda = \frac{\ln 2}{T_{1/2}} \quad (1)$$

A_0—Initial groundwater ^{14}C activity;
A_S—Measured ^{14}C activity of groundwater sample;
t—^{14}C age of the groundwater sample;
λ—^{14}C decay constant;
$T_{1/2}$—Half life of ^{14}C (5730 years).

The SCW samples had a ^{14}C activity of 24.9–47.7 pMC, with a median value of 40.3 pMC. The apparent age, the upper limit of the groundwater age, of the investigated water samples was calculated to provide a rough estimate of groundwater residence time.

The calculated ^{14}C apparent ages of the water samples are shown in Table 1S. The SCW has ^{14}C age ranges from 6100 to 11500 years, with an average value of 7700 years.

It can be seen in Fig. 6 that groundwater samples have a decreasing trend in TDS as the ^{14}C determined age increases, which indicates that the aquifers experienced many seawater transgressions, and are undergoing desalinization. The earlier the seawater intrusion occurs, the greater the degree of desalinization. Water samples with a high TDS (>20000 mg/L) cluster in the range of 6000 years, revealing that the study area experienced a large-scale seawater intrusion during that period. This observation is consistent with the descriptions given in section 2.

The groundwater salinity of the SCA is mainly the result of paleo-seawater intrusion of about 6000 years ago. However, Sr values and $^{87}Sr/^{86}Sr$ ratios (Fig. 5) suggest that other processes may have occurred.

5.2. Hydrochemical processes

As discussed above, the palaeo seawater intrusion dominates the characteristic of the SCW and this process is actually a mixture of fresh groundwater and the seawater. Therefore, it is necessary to address the issue of mixing.

A SCW sample (SC8) with the lowest TDS (366 mg/L), indicating that it was the least influenced by seawater, was chosen as the fresh water end-member. A sample of Yellow Sea water was chosen as the seawater end-member. The seawater mass fraction ($f_{mass,sea}$) of the SCW was calculated according to the conservative tracer Cl^- concentration using Eq. (2).

$$f_{mass,sea} = \frac{m_{Cl^-,sample} - m_{Cl^-,fresh}}{m_{Cl^-,sea} - m_{Cl^-,fresh}} \quad (2)$$

Where $m_{Cl^-,sample}, m_{Cl^-,fresh}, m_{Cl^-,sea}$ refers to the Cl^- concentration of groundwater samples, fresh water, and seawater, respectively.

By assuming conservative mixing, the theoretical concentration of each ion ($m_{i,mix}$) could be calculated by Eq. (3).

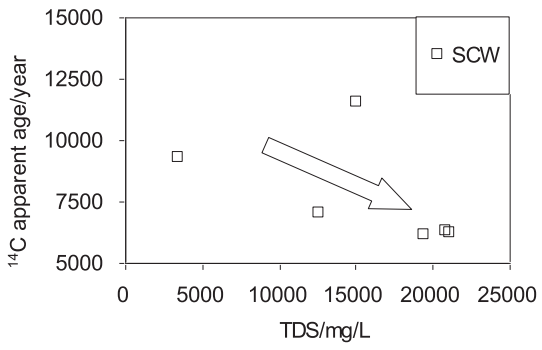

Fig. 6. Plot of TDS versus ^{14}C apparent age for the SCW.

$$m_{i,mix} = f_{mass,sea} \cdot m_{i,sea} + \left(1 - f_{mass,sea}\right) \cdot m_{i,fresh} \quad (3)$$

where $m_{i,sea}, m_{i,fresh}$ are the concentration of ion i of seawater and fresh water, respectively. The line of $m_{i,mix}$ vs Cl^- can then be calculated; this line was defined as the fresh/seawater mixing line (FSML) in this paper. The enrichment or depletion of ion i ($m_{i,rea}$) can be determined by Eq. (4).

$$m_{i,rea} = m_{i,sample} - m_{i,mix} \quad (4)$$

$m_{i,sample}$ refers to the concentration of ion i of a groundwater sample.

From Eq. (2), the seawater proportion was calculated as 0.07%–94.41%, with an average value of 45.61%. The seawater proportion of groundwater increases seaward along the flow path.

The groundwater samples in the plot of Cl^- versus Na^+, Mg^{2+}, and Br^- (Fig. 7 (a), (d), and (g), respectively) are aligned with the conservative mixing line between the fresh water end-member and Yellow Sea water, which further confirms that the salinity of the SCW results from mixing with seawater. However, in the plot of Cl^- vs. K^+, Ca^{2+}, SO_4^{2-}, HCO_3^- (Fig. 7 (b), (c), (e), (f), respectively), samples show an obvious deviation from the conservative mixing line. This indicates that the chemical compositions of the SCW are also affected by water-rock interactions.

5.2.1. Base exchange

The samples distribute above the mixing line in the plot of Cl^- vs. Ca^{2+} (Fig. 7(c)). The enrichment of Ca^{2+} could be affected by the dissolution of carbonate minerals and/or base exchange. However, the Ca^{2+} enrichment is well correlated with the K^++Na^+ depletion ($Ca^{2+}_{rea} = -0.74(K^+_{rea} + Na^+_{rea}) + 2.76$, $R = 0.88$, $n = 29$, Fig. 8(a)). The dissolution of carbonate minerals cannot account for K^++Na^+ depletion, which suggests that base exchange does occur. The SCA contains large amounts of clay particles with a high surface area and are thus very reactive in sorption and exchange processes (Clark, 2015).

Most samples show Ca^{2+} enrichment and K^++Na^+ depletion (Fig. 8(a)), suggesting that Na^+ in the SCW have been adsorbed to the solid phase after mixing with seawater (Eq. (5)).

$$2Na^+ + Ca - X_2 \rightarrow 2Na - X + Ca^{2+} \quad (5)$$

As shown in Fig. 8(b), $K^+_{rea} + Na^+_{rea}$ has little correlation with Mg^{2+}_{rea} (R = 0.12, n = 29), suggesting that the base exchange between $K^+_{rea} + Na^+_{rea}$ and Mg^{2+}_{rea} does not change the chemical composition of the groundwater.

The $^{87}Sr/^{86}Sr$ ratio of a mineral is controlled by its initial Rb/Sr ratio. Because Rb^+ can substitute for K^+, and Sr^{2+} can substitute for Ca^{2+}, potassium-bearing rocks will have high $^{87}Sr/^{86}Sr$ ratios (Negrel et al., 2001). Clay minerals typically have a high $^{87}Sr/^{86}Sr$ ratio (0.71030–0.72800) because of their high Rb/Sr ratio (Vengosh et al., 2002). When Ca-Na base exchange between groundwater and host clay minerals occurs during the fresh-saline water mixing process, Sr substitutes for Ca from the clay minerals, and desorbs to the water phase and increases the groundwater $^{87}Sr/^{86}Sr$ ratio. This process accounts for some water samples lying above the mixing zone in the plot of Sr^{2+} and $^{87}Sr/^{86}Sr$ (Fig. 5). However, water samples with the highest Sr^{2+} concentration, and high TDS values, have marine $^{87}Sr/^{86}Sr$ values (Fig. 5). This suggests that base exchange has little influence on the water chemistry of high TDS samples because of the limited adsorption sites of clay minerals.

5.2.2. Sulfate reduction and methanogenesis

Groundwater samples scatter below the mixing line in the plot

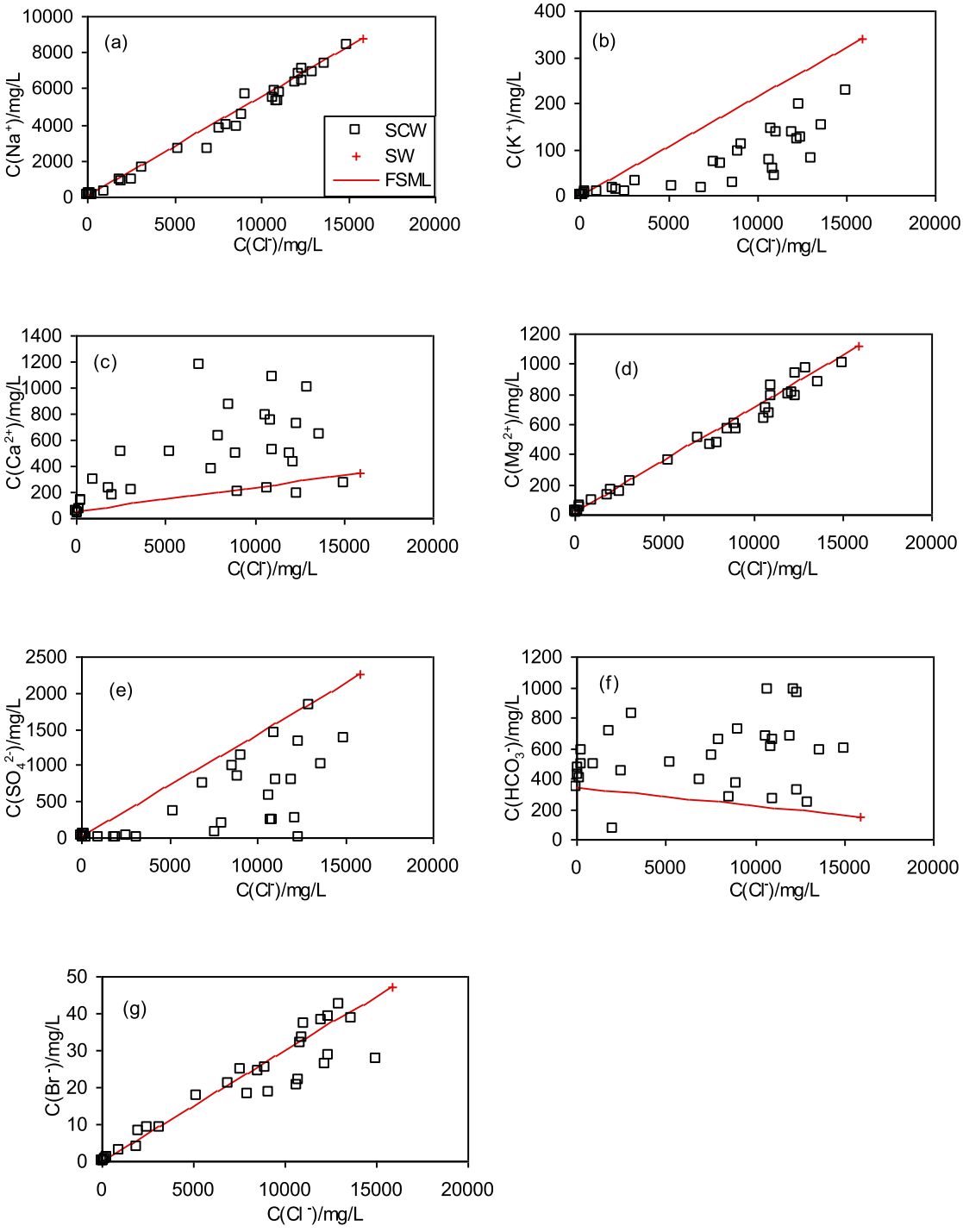

Fig. 7. Plots of Cl^- versus (a) Na^+; (b) K^+; (c) Ca^{2+}; (d) Mg^{2+}; (e) SO_4^{2-}; (f) HCO_3^-; and (g) Br^- (The FSML is shown by a red line). (For interpretation of the references to colour in this figure legend, the reader is referred to the web version of this article.)

of Cl^- vs. SO_4^{2-} (Fig. 7(e)). This may be the result of the precipitation of gypsum minerals and/or sulfate reduction. To test the assumption, the saturation index (SI) of groundwater samples with respect to gypsum and anhydrite were calculated and were all found to be below zero (Fig. 3S). This shows the groundwater samples are undersaturated with gypsum and anhydrite and that the gypsum minerals will not precipitate to reduce the concentration of sulfate. The groundwater samples plot above the mixing line in the plot of Cl^- vs. HCO_3^- (Fig. 7(f)) showing that the sulfate deficiency may be the result of sulfate reduction (Eq. (6)). Furthermore, $SO_4^{2-}{}_{rea}$ and $HCO_3^-{}_{rea}$ are negatively correlated ($HCO_3^-{}_{rea} = -0.30SO_4^{2-}{}_{rea} + 1.40$, R = 0.78, n = 29, Fig. 9(a)) which confirms the effect of sulfate reduction on sulfate depletion.

$$2CH_2O + SO_4^{2-} \rightarrow H_2S + 2HCO_3^- \quad (6)$$

In the process of sulfate reduction, sulfate is the electron acceptor during oxidizing the organic matter (Eq. (6)), and has a

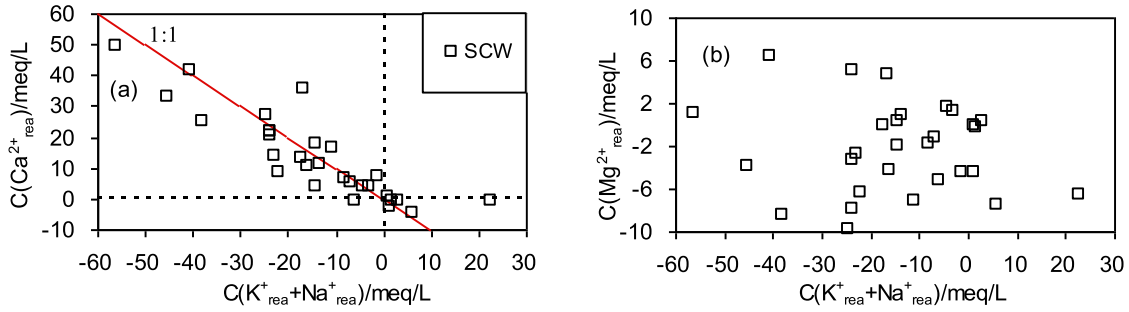

Fig. 8. Plot of $K^{+}_{rea} + Na^{+}_{rea}$ vs. (a) Ca^{2+}_{rea} and (b) Mg^{2+}_{rea} of SCW.

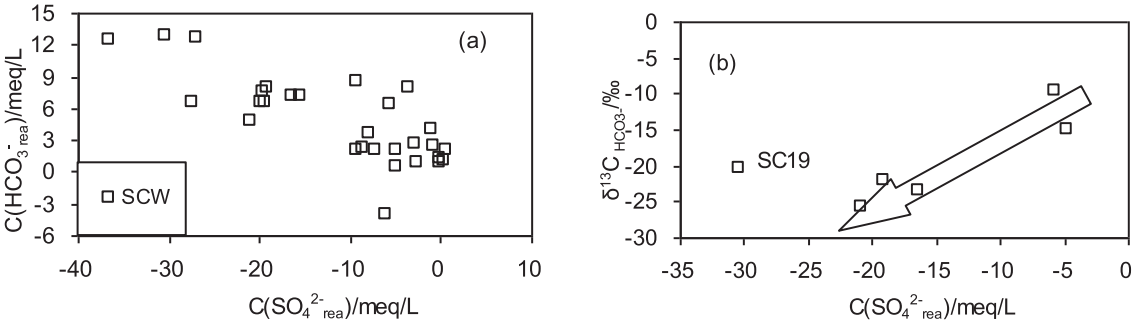

Fig. 9. Plots of $SO_4^{2-}{}_{rea}$ vs. (a) $HCO_3^{-}{}_{rea}$ and (b) $\delta^{13}C_{HCO3-}$ of SCW.

low $\delta^{13}C$ value of −25‰ to −30‰. During oxidation, ^{12}C reacts more easily than ^{13}C, resulting in the reaction product of HCO_3^- having a lower $\delta^{13}C$ value when compared with the organic matter (Clark and Fritz, 1997); the sulfate reduction reduces the $\delta^{13}C_{HCO3-}$ values of groundwater.

Fig. 9(b) shows that the $\delta^{13}C_{HCO3-}$ values of the groundwater samples decrease as $SO_4^{2-}{}_{rea}$ decreases. This further confirms the existence of sulfate reduction.

But SC19 sample is an exception. SC19 had a relatively low $SO_4^{2-}{}_{rea}$ concentration (−30.41 mg/L) but an enriched $\delta^{13}C_{HCO3-}$ value of −20.4‰ (Fig. 9(b)), which may due to the methanogenesis process. When O_2, NO_3^-, and SO_4^{2-} are absent in groundwater, bacteria will consume carbon to produce CO_2 and CH_4 (the methanogenesis process). This process has two main components: acetate fermentation (Eq. (7)) and CO_2 reduction (Eq. (8)). Both components of the process cause $\delta^{13}C_{HCO3-}$ values to rise because of the large ^{13}C fractionation between CO_2 and CH_4 (20–50% for acetate fermentation and 60–80% for CO_2 reduction (Cartwright, 2010; Clark and Fritz, 1997)).

$$2CH_2O \rightarrow CO_2 + CH_4 \quad (7)$$

$$CO_2 + 4H^+ \rightarrow CH_4 + 2H_2O \quad (8)$$

5.2.3. Equilibrium of carbonate minerals

If the concentration of Ca^{2+} is dominated by base exchange with K^+ and Na^+, the $Ca^{2+}{}_{rea}/(K^+{}_{rea} + Na^+{}_{rea})$ ratio should be close to 1. If the concentration of HCO_3^- is dominated by sulfate reduction, the $HCO_3^-{}_{rea}/SO_4^{2-}{}_{rea}$ ratio should also be close to 1. However, the two ratios are all less than 1, with a $Ca^{2+}{}_{rea}/(K^+{}_{rea} + Na^+{}_{rea})$ ratio of about 0.74 and a $HCO_3^-{}_{rea}/SO_4^{2-}{}_{rea}$ ratio of about 0.30. Therefore, other reactions must be taking place to cause the Ca^{2+} depletion. Furthermore, most of the groundwater samples show a depletion of Mg^{2+} (Fig. 8(b)). It is suggested that the precipitation of carbonate minerals is a reasonable explanation for Ca^{2+}, Mg^{2+}, and HCO_3^- depletion. The SI of groundwater samples with respect to calcite and dolomite were calculated. The results show that the SI for

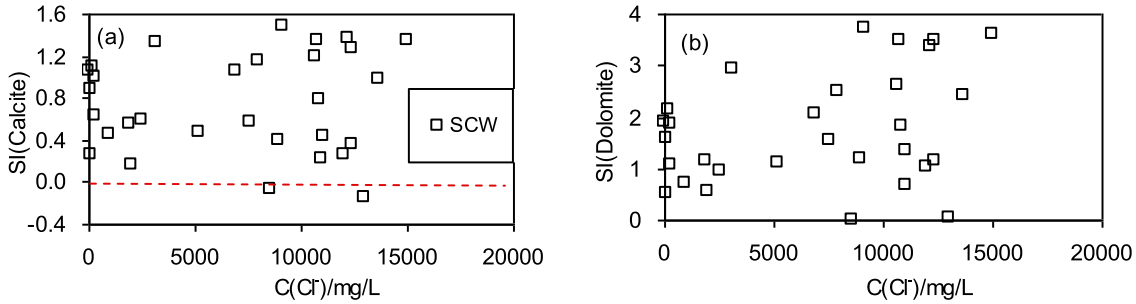

Fig. 10. Plots of Cl^- concentration vs. SI of (a) calcite, and (b) dolomite.

calcite and dolomite for most groundwater samples was greater than zero, indicating that calcite and dolomite are oversaturated in the investigated groundwater samples (Fig. 10). Thus, calcite and dolomite tend to precipitate to decrease the Ca^{2+}, Mg^{2+}, and HCO_3^- concentrations.

6. Conclusions

We combined different methods and tracers to study the origins of groundwater salinity and hydrogeochemical processes in the SCA in the coastal plain north of the Yangtze River, China. The shallow confined water is mainly composed of salt water. The TDS of the aquifer increases from below 500 mg/L in the inland area to more than 20000 mg/L around the coastline. The water type evolves from HCO_3-Ca to Cl-Na as TDS increases. Enrichment with $\delta^{18}O$, δD, marine-like $^{87}Sr/^{86}Sr$ values, and high iodine concentrations suggest that groundwater salinity originates from paleo-seawater intrusions. The analyses of ^3H and ^{14}C revealed that most of the groundwater salinity originated from a seawater transgression around 6000 years ago. The seawater proportions in the groundwater samples ranged from 0.07% to 94.41%, and exhibited the same spatial distribution pattern as TDS.

In addition to mixing with seawater, the chemical composition of the SCW is affected by water-rock interactions, which have an influence on K^+, Na^+, Mg^{2+}, and SO_4^{2-} depletion and Ca^{2+}, HCO_3^- enrichment. Analyses involving a mass balance mixing model, ionic relationships, $^{87}Sr/^{86}Sr$ ratios, ^{13}C values, and saturation indices were used to further investigate the processes involved. The changes in K^+, Na^+, and Ca^{2+} are caused by base exchange process. The changes in SO_4^{2-} and HCO_3^- are the result of sulfate reduction and methanogenesis. Saturation indices greater than zero indicate that carbonate equilibrium processes have had some effect on Ca^{2+}, Mg^{2+}, and HCO_3^- concentrations.

Salt water can be used in agricultural irrigation, seafood farming, and industry, for example, and thereby reduce the use of deep confined fresh water. In addition, using the shallow confined salt water will lower the water table and accelerate the desalinization process. Therefore, the exploitation of shallow confined salt water should be considered in future water management plans. In addition to guiding future management plans, this study provides useful insights for other studies in similar regions.

Acknowledgements

This work was funded by the Groundwater Circulation and Water Chemical Evolution Project of the Jiangsu Coastal Area ([2012]01-002-007), which is a branch project of the Comprehensive Geological Survey of the Jiangsu Coastal Area (a key cooperation project of the Jiangsu Provincial People's Government and the Ministry of Land and Resources). The authors thank the Geological Survey of Jiangsu Province for assistance with the study's fieldwork and for supplying basic hydrogeological information. We thank Liwen Bianji, Edanz Group China (www.liwenbianji.cn), for editing the English text of a draft of this manuscript.

Appendix A. Supplementary data

Supplementary data related to this article can be found at https://doi.org/10.1016/j.apgeochem.2017.09.015.

References

Bakari, S.S., Aagaard, P., Vogt, R.D., Ruden, F., Johansen, I., Vuai, S.A., 2013. Strontium isotopes as tracers for quantifying mixing of groundwater in the alluvial plain of a coastal watershed, south-eastern Tanzania. J. Geochem Explor 130, 1–14.

Boschetti, T., Toscani, L., Shouakar-Stash, O., Iacumin, P., Venturelli, G., Mucchino, C., Frape, S.K., 2010. Salt waters of the northern apennine foredeep basin (Italy): origin and evolution. Aquat. Geochem 17, 71–108.

Brenot, A., Négrel, P., Petelet-Giraud, E., Millot, R., Malcuit, E., 2015. Insights from the salinity origins and interconnections of aquifers in a regional scale sedimentary aquifer system (Adour-Garonne district, SW France): contributions of $\delta^{34}S$ and $\delta^{18}O$ from dissolved sulfates and the 87Sr/86Sr ratio. Appl. Geochem 53, 27–41.

Cartwright, I., Weaver, T., Petrides, B., 2007. Controls on $^{87}Sr/^{86}Sr$ ratios of groundwater in silicate-dominated aquifers: SE Murray Basin, Australia. Chem. Geol. 246, 107–123.

Cartwright, I., 2010. Using groundwater geochemistry and environmental isotopes to assess the correction of ^{14}C ages in a silicate-dominated aquifer system. J. Hydrol. 382, 174–187.

Cary, L., Petelet-Giraud, E., Bertrand, G., Kloppmann, W., Aquilina, L., Martins, V., Hirata, R., Montenegro, S., Pauwels, H., Chatton, E., Franzen, M., Aurouet, A., Team, 2015. Origins and processes of groundwater salinization in the urban coastal aquifers of Recife (Pernambuco, Brazil): a multi-isotope approach. Sci. Total Environ. 530–531, 411–429.

Chandrajith, R., Chaturangani, D., Abeykoon, S., Barth, J.A.C., van Geldern, R., Edirisinghe, E.A.N.V., Dissanayake, C.B., 2013. Quantification of groundwater–seawater interaction in a coastal sandy aquifer system: a study from Panama, Sri Lanka. Environ. Earth Sci. 72, 867–877.

Clark, I., Fritz, P., 1997. Environmental Isotopes in Hydrogeology (Lewis, New York).

Clark, I., 2015. Groundwater Geochemistry and Isotopes. CRC Press, Boca Raton, Florida.

Colombani, N., Cuoco, E., Mastrocicco, M., 2017. Origin and pattern of salinization in the Holocene aquifer of the southern Po Delta (NE Italy). J. Geochem Explor 175, 130–137.

Custodio, E., 2010. Coastal aquifers of Europe: an overview. Hydrogeol. J. 18, 269–280.

de Montety, V., Radakovitch, O., Vallet-Coulomb, C., Blavoux, B., Hermitte, D., Valles, V., 2008. Origin of groundwater salinity and hydrogeochemical processes in a confined coastal aquifer: case of the Rhône delta (Southern France). Appl. Geochem 23, 2337–2349.

Edmunds, W.M., 2001. Paleowaters in European Coastal Aquifers – the Goals and Main Conclusions of the PALAEAUX Project, vol. 189. Geological Society, London, pp. 1–16. Special Publications.

Eissa, M.A., Thomas, J.M., Pohll, G., Shouakar-Stash, O., Hershey, R.L., Dawoud, M., 2016. Groundwater recharge and salinization in the arid coastal plain aquifer of the Wadi Watir delta, Sinai, Egypt. Appl. Geochem 71, 48–62.

Ghabayen, S.M.S., McKee, M., Kemblowski, M., 2006. Ionic and isotopic ratios for identification of salinity sources and missing data in the Gaza aquifer. J. Hydrol. 318, 360–373.

Hamouda, M.F.B., Tarhouni, J., Leduc, C., Zouari, K., 2011. Understanding the origin of salinization of the Plio-quaternary eastern coastal aquifer of Cap Bon (Tunisia) using geochemical and isotope investigations. Environ. Earth Sci. 63, 889–901.

Han, D.M., Kohfahl, C., Song, X.F., Xiao, G.Q., Yang, J.L., 2011. Geochemical and isotopic evidence for paleo-seawater intrusion into the south coast aquifer of Laizhou Bay, China. Appl. Geochem 26, 863–883.

Herczeg, A.L., Dogramaci, S.S., Leaney, F.W.J., 2001. Origin of dissolved salts in a large, semi-arid groundwater system: MDB, Australia. Mar. Freshw. Res. 52, 41.

Hofmann, H., Cartwright, I., 2013. Using hydrogeochemistry to understand inter-aquifer mixing in the on-shore part of the Gippsland Basin, southeast Australia. Appl. Geochem 33, 84–103.

Jørgensen, N.O., Andersen, M.S., Engesgaard, P., 2008. Investigation of a dynamic seawater intrusion event using strontium isotopes (87Sr/86Sr). J. Hydrol. 348, 257–269.

Khaska, M., Salle, C.L.G.L., Lancelot, J., Team, A., Mohamad, A., Verdoux, P., Noret, A., Simler, R., 2013. Origin of groundwater salinity (current seawater vs. saline deep water) in a coastal karst aquifer based on Sr and Cl isotopes. Case study of the La Clape massif (southern France). Appl. Geochem 37, 212–227.

Li, J., Wang, Y., Xie, X., 2016. Cl/Br ratios and chlorine isotope evidences for groundwater salinization and its impact on groundwater arsenic, fluoride and iodine enrichment in the Datong basin, China. Sci. Total Environ. 544, 158–167.

Mongelli, G., Monni, S., Oggiano, G., Paternoster, M., 2013. Tracing groundwater salinization processes in coastal aquifers: a hydrogeochemical and isotopic approach in Na-Cl brackish waters of north-western Sardinia, Italy. Hydrol. Earth Syst. Sci. 17, 2917–2928.

Moran, J.E., Oktay, S.D., Santschi, P.H., 2002. Sources of iodine and iodine 129 in rivers. Water Resour. Res. 38, 24–21-24-10.

Moussa, A.B., Zouari, K., Marc, V., 2011. Hydrochemical and isotope evidence of groundwater salinization processes on the coastal plain of Hammamet–Nabeul, north-eastern Tunisia. Phys Chem Earth 36, 167–178.

Negrel, P., Casanova, J., Aranyossy, J.F., 2001. Strontium isotope systematics used to decipher the origin of groundwaters sampled from granitoids: the Vienne Case (France). Chem. Geol. 177, 287–308.

Petelet-Giraud, E., Negrel, P., Aunay, B., Ladouche, B., Bailly-Comte, V., Guerrot, C., Flehoc, C., Pezard, P., Lofi, J., Dorfliger, N., 2016. Coastal groundwater salinization: focus on the vertical variability in a multi-layered aquifer through a multi-isotope fingerprinting (Roussillon Basin, France). Sci. Total Environ. 566–567, 398–415.

Rozanski, K., Araguás-Araguás, L., Gonfiantini, R., 1993. Isotopic Patterns in Modern Global Precipitation. Climate Change in Continental Isotopic Records. American Geophysical Union Monograph, pp. 1–36.

Santucci, L., Carol, E., Kruse, E., 2016. Identification of paleo-seawater intrusion in

groundwater using minor ions in a semi-confined aquifer of the Rio de la Plata littoral (Argentina). Sci. Total Environ. 566–567, 1640–1648.
Shi, L., Jiao, J.J., 2014. Seawater intrusion and coastal aquifer management in China: a review. Environ. Earth Sci. 72, 2811–2819.
Sukhija, B.S., Varma, V.N., Nagabhushanam, P., Reddy, D.V., 1996. Differentiation of paleomarine and modern seawater intruded salinities in coastal groundwaters (of Karaikal and Tanjavur, India) based on inorganic chemistry, organic biomarker fingerprints and radiocarbon dating. J. Hydrol. 174, 173–201.
Szynkiewicz, A., Modelska, M., Medina, M.R., Farmer, G.L., Rabago, P.H., Monreal, R., 2014. Age and shape of paleo-seawater intrusions in the semi-arid coastal aquifer of Sonora Desert, northern Mexico. Geosci. Notes 2, 11–38.
Trabelsi, R., Zairi, M., Dhia, H.B., 2007. Groundwater salinization of the Sfax superficial aquifer, Tunisia. Hydrogeol. J. 15, 1341–1355.
van Geldern, R., Baier, A., Subert, H.L., Kowol, S., Balk, L., Barth, J.A., 2014. Pleistocene paleo-groundwater as a pristine fresh water resource in southern Germany—evidence from stable and radiogenic isotopes. Sci. Total Environ. 496, 107–115.
Vengosh, A., Gill, J., Lee Davisson, M., Bryant Hudson, G., 2002. A multi-isotope (B, Sr, O, H, and C) and age dating (^{3}H-^{3}He and^{14}C) study of groundwater from Salinas Valley, California: hydrochemistry, dynamics, and contamination processes. Water Resour. Res. 38, 9–1-9-17.
Wang, Y., Jiao, J.J., 2012. Origin of groundwater salinity and hydrogeochemical processes in the confined Quaternary aquifer of the Pearl River Delta, China. J. Hydrol. 438–439, 112–124.
Werner, A.D., Bakker, M., Post, V.E.A., Vandenbohede, A., Lu, C., Ataie-Ashtiani, B., Simmons, C.T., Barry, D.A., 2013. Seawater intrusion processes, investigation and management: recent advances and future challenges. Adv. Water Res. 51, 3–26.
WHO, 2011. Guidelines for Drinking-water Quality, fourth ed., p. 398
Yechieli, Y., Kafri, U., Sivan, O., 2008. The inter-relationship between coastal subaquifers and the Mediterranean Sea, deduced from radioactive isotopes analysis. Hydrogeol. J. 17, 265–274.
Zhang, E., Wang, Y., Qian, Y., Ma, T., Zhang, D., Zhan, H., Zhang, Z., Fei, Y., Wang, S., 2013. Iodine in groundwater of the North China Plain: spatial patterns and hydrogeochemical processes of enrichment. J. Geochem Explor 135, 40–53.